Szke, M., & Azarpeyvand, M. (2016). Trailing edge noise measurement: assumptions and uncertainties. Paper presented at 23rd International Congress on Sound and Vibration, Athens, Greece.

Peer reviewed version

PDF-document

University of Bristol - Explore Bristol Research
General rights

TRAILING EDGE NOISE MEASUREMENT: ASSUMPTIONS AND UNCERTAINTIES

Máté Szőke and Mahdi Azarpeyvand

Aerodynamics and Aeroacoustics Research Group, University of Bristol,
Queens Building, University Walk, Bristol, BS8 1TR, United Kingdom
email: m.szoke@bristol.ac.uk

This study aims to investigate the assumptions used in analytical models for the prediction of trailing edge noise and uncertainties involved in the measurement of near-field flow parameters, such as surface pressure spectra, convection velocity and spanwise length scale. The comparison and accuracy analysis of several aerofoil trailing edge noise models is performed. The study investigates the models developed by Amiet, Parchen (TNO) and Brooks-Pope-Marcolini (BPM). To provide the input variables for the different models, a flat plate has been manufactured on which the surface pressure fluctuations are measured using an array of flush mounted microphones and the boundary layer properties are found using hot-wire probes. It was found that the input properties of the investigated trailing edge noise prediction models showed strong dependency on the trailing edge condition and that the far-field noise predictions can be significantly affected by these changes.

1.   Introduction

Trailing edge noise is one of the main components of aerofoil self-noise [1, 2]. The phenomena plays an important role in the noise generation in the field of aviation, wind turbines, turbo-machinery, etc. The main cause of the noise is the pressure fluctuations over the surface generated by turbulence which is being scattered to the far field from the trailing edge (TE). The mechanism of the TE generated noise has been a topic of research interest over several decades.

The problem has been addressed both by measurements and mathematical modelling, from which we can now find empirical, semi-empirical, and analytical models to predict the TE noise [3, 4, 5, 6]. These models predict the noise by relying on the properties of turbulence and the boundary layer which are mainly calculated from upstream geometry and flow conditions. The main input parameters of these models are, for example, the surface pressure fluctuation, turbulence length scales, convection velocity and boundary layer displacement thickness, etc.

Based on the developed models, several attempts have been made to reduce the noise both by modifying the flow over the surface or by changing the geometry [7, 8, 9]. These have been addressed by measurements in anechoic chambers and using computational methods, both of which are limited by their own constraints [10, 11, 12]. Capturing the low frequency components of the scattered noise is difficult due to the background jet noise in anechoic wind tunnels and the finite size of the anechoic chambers. From the computational side, resolving the pressure fluctuations over a wide range of frequencies due to the broadband nature of the TE noise is necessary, which causes inevitable difficulties for fluid flow solvers. These limitations increase the uncertainty in the exact resolution of the TE noise, which means that the accurate description of the noise is more difficult in these "shadow zones". For this reason, the better understanding of the uncertainties of the TE models is necessary.

The developed TE noise models reduce the complexity of the mathematical description of the fluid flow by adapting different assumptions (frozen turbulence, two dimensionality, isotropic turbulence etc.), which are valid either in a given range of applications or in specific conditions. One of the most important effects which distorts the flow is the presence of the TE itself by introducing a singularity and discontinuity in the geometrical condition of the flow. This condition, and especially when it presents alongside with adverse pressure gradient (e.g. aerofoils), can change the flow upstream of the TE such that the assumptions considered by the different TE noise models might not be valid any more. The effect of the TE without the presence of adverse pressure gradient in the flow is considered in the current paper by measuring the turbulence properties above an extendible flat plate. The plate offers the opportunity to perform measurements of velocity and surface pressure fluctuations at given streamwise locations with and without the presence of a TE.

This paper is organised as follows: Section 2 gives an overview on how the measurement of the trailing edge boundary layer was performed in order to capture the hydrodynamic field related quantities relevant to the TE noise prediction models. These models with their main assumptions and input parameters are briefly presented in Section 3. Finally, the effects of the presence of trailing edge on the measured quantities are shown and discussed in Section 4.
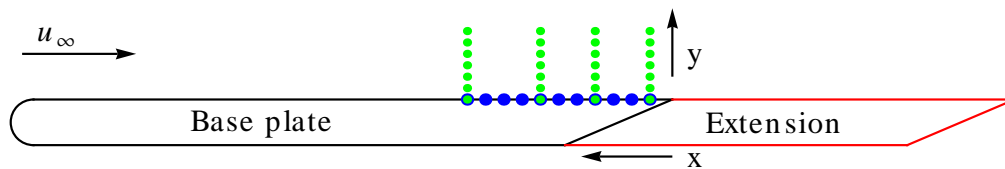
2. Measurement Set-up

Figure 1: The schematic of the rig: base plate (black); extension (red); microphone locations (blue); velocity measurement locations (green)

A flat plate was built to measure the flow properties, see Fig. 1. The rig consists of a base plate and an extension component which can be attached to the base plate so that it can be extended further downstream. The TE is made of a 12° sharp wedge and the location of the TE can be shifted downstream using the extension component. The width of the rig is $L = 715$ mm, the length of the plate is 1000 mm and it is 1500 mm long with the extension component.

Measurements were carried out in the open test section return type wind tunnel of the University of Bristol, in which the far field flow velocity was set to $u_\infty = 10$ m/s with a typical turbulence intensity of less than 1 %. The properties of the flow was measured with Dantec 55P16 type miniature hot-wire, which was operated by Dantec 91C10 CTA modules at an overheat ratio of 1.8. The uncertainty of the hot-wire measurements was found to be less than ± 0.5 %. The surface pressure fluctuations were measured at 24 different streamwise and spanwise locations with Knowles FG-23329-P07 type miniature electret condenser microphones, which were calibrated in advance of the measurements. The data acquisition system was National Instruments PXIe-4499 type operated with a sampling frequency and measurement time of $65536 = 2^{16}$ Hz and 8 sec. During the post processing of the measured quantities, the frequency resolution was set to 64 Hz for all quantities that are defined in the frequency domain.

Using the velocity ($u(x,t)$) and pressure ($p(x,t)$) data collected, a set of physical properties can be calculated, which gives a basis to study the changes to the turbulence properties of the flow for the two investigated geometrical conditions. The calculated properties are the followings: mean velocity ($\bar{u}$), root mean square of velocity (u_{RMS}), friction velocity (u_τ, found iteratively from the boundary layer velocity measurement results), boundary layer thickness (δ, defined where the velocity profile reaches 99 % of the free-stream velocity u_∞), boundary layer displacement thickness (δ^*), boundary

layer momentum thickness (θ), point spectra of surface pressure fluctuations (ϕ_{pp}), Pearson's correlation coefficient (r) defined between velocity (u') and pressure (p') fluctuations [13], magnitude squared coherence (γ^2) between u' and p', spanwise turbulence length scale (Λ_3) and temporal cross correlation ($R_{u'p'}$).

3. Trailing Edge Noise Models

The current paper investigates three different TE noise models, namely, the BPM [5], Amiet [3] and Parchen's TNO [4] trailing edge noise models and their most important inputs. These models are presented in this section, where the main input properties are highlighted for each model and the parameters for which the presence of the TE has no or negligible effect are also listed.

3.1 BPM Model

The BPM model is an empirical model developed by Brooks, Pope and Marcolini [5] based on several aerofoil noise measurements. The far field sound pressure level generated by an aerofoil is defined as

$$S(f) = 10 \log \left(\frac{\delta^* M^5 L D_h}{R^2} \right) + A \left(\frac{St_\delta}{St_1} \right) + K_1 - 3, \tag{1}$$

where $St_\delta = (f\delta^*)/u_\infty$, $St_1 = 0.02M^{-0.6}$, M is the Mach number, K_1 is an empirical constant which is a function of angle of attack, $D_h = (2\sin^2(\Theta/2)\sin^2(\Phi))/((1 + M\cos\Theta)[1 + (M - M_c)\cos\Theta])$, in which Φ, Θ and R are describing the location of the observer, $M_c = 0.8M$ is the convection Mach number and A is the empirical spectral shape parameter which is defined as function of Strouhal number ratio. A more detailed description can be found in [3].

We can see that L, M, A, K_1, R and the fluid properties are not affected by the presence of the TE for a fixed observer location and far field velocity, while δ^* and M_c might be affected by the presence of the TE. Therefore, the changes to the boundary layer displacement thickness (δ^*) and the convection velocity (u_c) will be investigated experimentally.

3.2 TNO Model

The TNO model was developed by Parchen [4] is a semi-empirical model, assuming frozen and isotropic turbulence. The model integrates the surface pressure fluctuation over the entire wavenumber domain in the streamwise direction to achieve the far-field pressure power spectra. The surface pressure spectra as a function of wavenumber, $\mathbf{k} = (k_1, k_2, k_3)$, and frequency reads as

$$\phi_{pp}(\mathbf{k}, \omega) = 4\varrho^2 \frac{k_1^2}{k_1^2 + k_3^2} \int_0^\infty L_2(y) \bar{u}_2^2 \left(\frac{\partial u}{\partial y} \right)^2 \phi_{22}(\mathbf{k}, \omega) \phi_m(\omega - u_c(y)k_1) e^{-2|k||y_2|} \mathrm{d}y, \tag{2}$$

where ϕ_m is the so called moving axis spectrum that is dedicated to define the distortion of turbulent eddies as they pass over the TE and ϕ_{22} is the spectrum of the vertical velocity fluctuations. These quantities are defined in the model as:

$$\phi_m(\omega - u_c(y)k_1) = \frac{1}{\alpha_G\sqrt{\pi}} e^{-[(\omega - u_c(y)k_1)/\alpha_G]^2}, \tag{3}$$

$$\phi_{22}(k_1, k_3) = \frac{4}{9\pi k_e^2} \frac{(k_1/k_e)^2 + (k_3/k_e)^2}{[1 + (k_1/k_e)^2 + (k_3/k_e)^2]^{7/3}}, \tag{4}$$

where $k_e \approx 0.74/L_2$ is the wavenumber of the energy containing eddies, $\alpha_G = 0.05u_c/L_2$ is the Gaussian constant and $u_c = 0.7u_\infty$ is the convection velocity. Finally, the far-field sound pressure

reads as

$$S(\omega) = \frac{L}{4\pi R^2} \int\limits_{-\infty}^{\infty} \frac{\omega}{c_0 k_1} \, \phi_{pp}(\mathbf{k}, \omega)|_{k_3=0} \, \mathrm{d}k_1. \tag{5}$$

Similarly as in the former case, L, R are independent of the flow condition and are not affected by the TE. The presence of a TE may, however cause some changes to the convection velocity (u_c), the shear stress in the boundary layer ($\partial u/\partial y$), the vertical integral length scale of turbulent eddies ($L_2(y_2)$) and the vertical velocity fluctuation ($\bar{u}_2^2$), which can effect the surface pressure spectrum (ϕ_{pp}). Therefore, the measurements are focused on the resolution of these properties.

3.3 Amiet Model

The analytical TE noise model which was developed by Amiet [3] also gives a connection between the surface pressure fluctuation and the far-field pressure power spectra. The model assumes frozen turbulence and large span to chord ratio ($c >> L$). The far-field pressure power spectra (S_{pp}) and the radiation integral ($\mathcal{L}$) are defined as

$$S_{pp}(x, y, z, \omega) = \frac{\omega c y}{4\pi c_0 \sigma^2} \frac{L}{2} |\mathcal{L}|^2 \Lambda_z(\omega) \phi_{pp}(\omega, 0), \tag{6}$$

$$|\mathcal{L}| = \frac{1}{\Theta} \left| (1+i) \left\{ \sqrt{\frac{1 + M + \bar{K}_x/\mu}{1 + x/\sigma}} E^* \left[2\mu(1 + x/\sigma) \right] \mathrm{e}^{-2i\Theta} - E^* \left[2((1+M)\mu + \bar{K}_x) \right] \right\} + 1 \right|. \tag{7}$$

The convection of acoustic waves is defined as $\sigma^2 = x^2 + \beta^2 y^2$, where $\beta^2 = 1 - M^2$, $M = u_\infty/c_0$ is the Mach number and c_0 is the speed of sound. Also, $\Theta = \bar{K}_x + \mu(M - x/\sigma)$, $\bar{K}_x = \omega/u_c$, and $\mu = M\omega b/(u\beta^2)$. Finally, $E^*(x)$ denotes Fresnel integrals, which is defined as

$$E^*(x) = \int\limits_0^x \frac{-\mathrm{i}\xi}{\sqrt{2\pi\xi}}. \tag{8}$$

According to the model, the surface pressure spectra in the mid plane can be calculated as

$$\phi_{pp}(\omega, 0) = \frac{4\pi \varrho_0^2}{\Lambda_3(\omega)} \int\limits_0^\delta \Lambda_2(y) \left(\frac{\partial u}{\partial y} \right)^2 \bar{u}_2^2(y) \phi_{22}(\omega - u_c(y)k_1) \mathrm{e}^{-2|k|y} \mathrm{d}y, \tag{9}$$

from which one can conclude that the parameters used in the TNO model also influence the accuracy of the Amiet model. An additional term is present in the Amiet model which is the spanwise length scale of the turbulent eddies (Λ_3),

$$\Lambda_3(\omega) = \int\limits_0^\infty \sqrt{\gamma^2(\omega, \Delta z)} \mathrm{d}\Delta z, \tag{10}$$

where γ^2 is the magnitude square coherence between measured surface pressure fluctuations and Δz is the distance between two microphones.

4. Measurement Results

In this section the results from the measurements will be introduced and discussed. The following figures are comparing the results from the two investigated layouts which are referred to as the TE and the no TE cases in the discussion. Throughout this section, the red dashed and the black solid

(a) at $x = 4.5$ mm   (b) at $x = 14.6$ mm   (c) at $x = 72$ mm   (d) at $x = 92$ mm
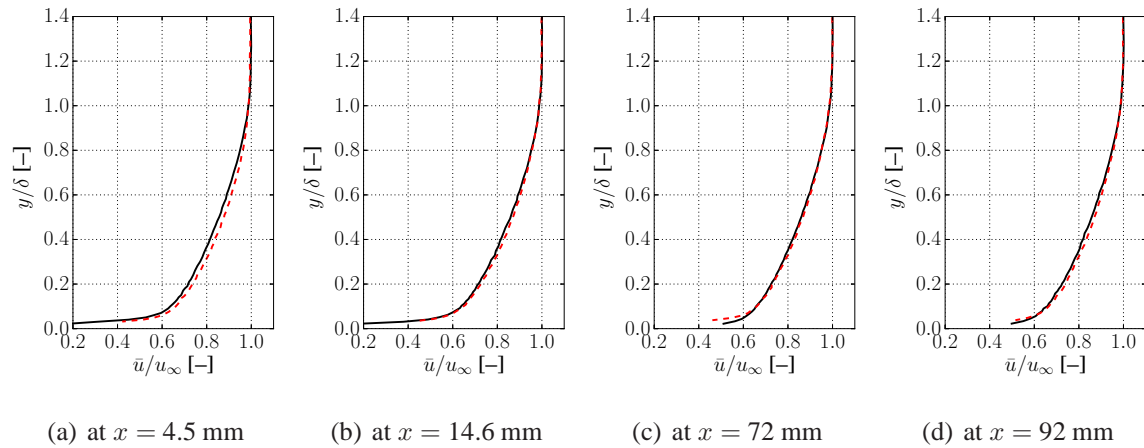
Figure 2: Boundary layer mean velocity profiles at different streamwise locations upstream of the trailing edge; – no TE case, – – TE case

lines show, respectively, the results for the TE and no TE (*i.e.* standard boundary layer) cases. Results will be presented at four locations, above the surface pressure microphones located at $x = 4.5$, 14.6, 72 and 92 mm upstream of the TE.

The boundary layer behaviour upstream of the TE is shown in Fig. 2. The effect of the discontinuity is noticeable for the location near the TE ($x = 4.5$ and 14.6 mm), while the difference fades away further upstream ($x = 72$ and 92 mm). It is also observed for the measurement near the TE that the BL velocity profile has a different gradient to that of the no TE case, see Fig. 2(a). This indicates that the presence of the TE discontinuity causes more friction upstream and in the vicinity of the TE. This component can be identified as $\partial u / \partial y$ in the TE noise models, see Section 3. Additional measurements are planned involving surface mounted hot-film sensors to further investigate this phenomena.

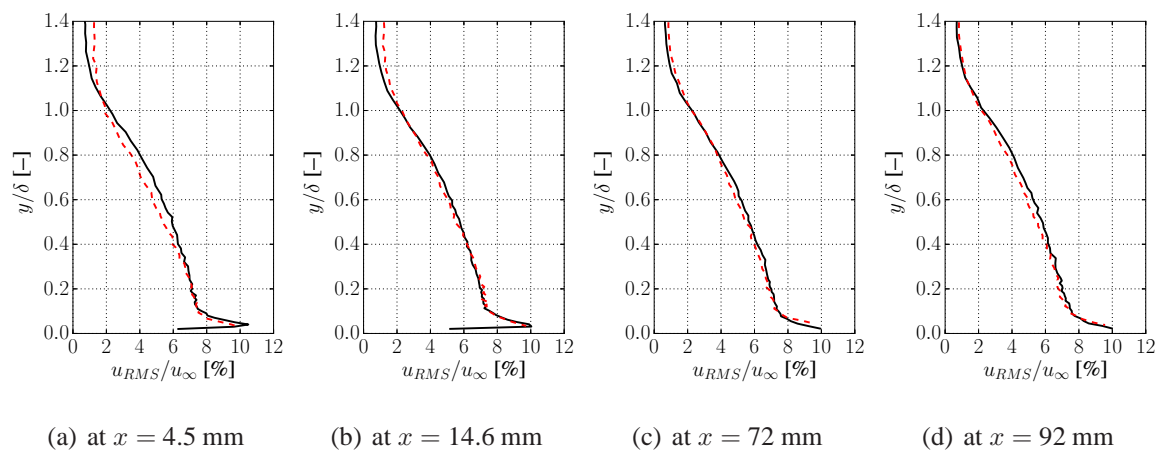(a) at $x = 4.5$ mm   (b) at $x = 14.6$ mm   (c) at $x = 72$ mm   (d) at $x = 92$ mm

Figure 3: Boundary layer RMS velocity profiles at different streamwise locations upstream of the trailing edge; – no TE case, – – TE case

The energy content of the turbulent structures within the BL can be studied using the RMS velocity results. Figure 3 shows the u_{RMS} at different streamwise location for the TE and no TE cases. By comparing the results, one can conclude that the energy content in the BL does not change significantly at upstream locations, until in the close vicinity of the TE ($x = 4.5$ mm) where the energy content of the boundary layer decreases between $y/\delta = 0.4$ and the edge of the BL. This shows that the flow within the BL, and in particular in the outer layer of the BL, changes as it approaches the TE.

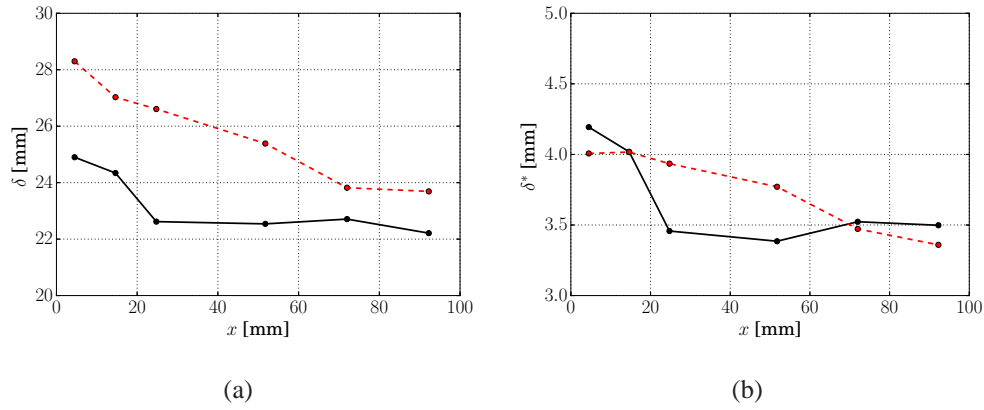(a)   (b)

Figure 4: Further boundary layer properties upstream of the trailing edge I: (a) boundary layer thickness, (b) boundary layer displacement thickness along the streamwise coordinate upstream of the trailing edge; – no TE case, – – TE case

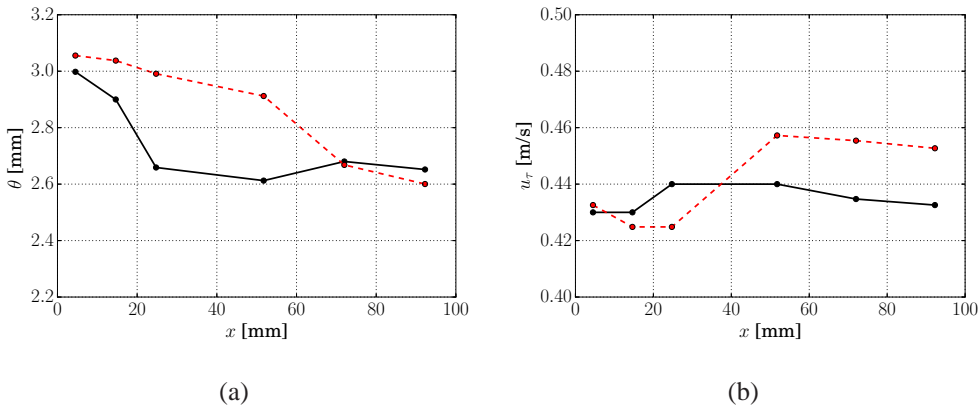(a)   (b)

Figure 5: Further boundary layer properties upstream of the trailing edge II: (a) boundary layer momentum thickness and (b) friction velocity along the streamwise coordinate upstream of the trailing edge; – no TE case, – – TE case

Other flow properties such as the boundary layer thickness (δ), displacement thickness (δ^*), momentum thickness (θ) and friction velocity (u_τ) are plotted in Figs. 4 and 5. As seen before, the discrepancy between the two geometrical cases increases as we move closer to the TE location. The integral properties $(\delta^*$ and $\theta)$ of the boundary layer profile show this behaviour too. This also indicates the distortion of the boundary layer in the presence of the TE. Figure 5(b) shows the friction velocity, which was found iteratively at each streamwise location by achieving the smallest difference between the measurements and the logarithmic wall law in the region of $y^+ \in (90, 200)$. The baseline case which is presented by black solid line shows a reasonably stable friction velocity along the streamwise coordinate, unlike the case when the TE is present in the flow. In the latter case, the friction velocity decreases as we approach the TE. This property is related to $(\partial u / \partial y)_{y=0}$ (see Section 3), which is an important parameter in the TNO and Amiet TE noise models. This phenomena together with the changes in all of the formerly presented variables show that the frozen turbulence approach is not valid in the vicinity of the TE even without the presence of adverse pressure gradient.

Besides the time-averaged quantities, reviewed above, the frequency-energy content of the BL quantities and the surface pressure fluctuations also play a very important role in the prediction of the TE noise. While in this paper the point spectra of the pressure fluctuation is presented $(\phi_{pp}(f))$, further measurements are planned in order to capture the pressure fluctuations in the wavenumber (spatial) domain as well. Figure 6 shows $\phi_{pp}(f)$ at the same axial (x) locations as before. The peaks

(a) at $x = 4.5$ mm

(b) at $x = 14.6$ mm
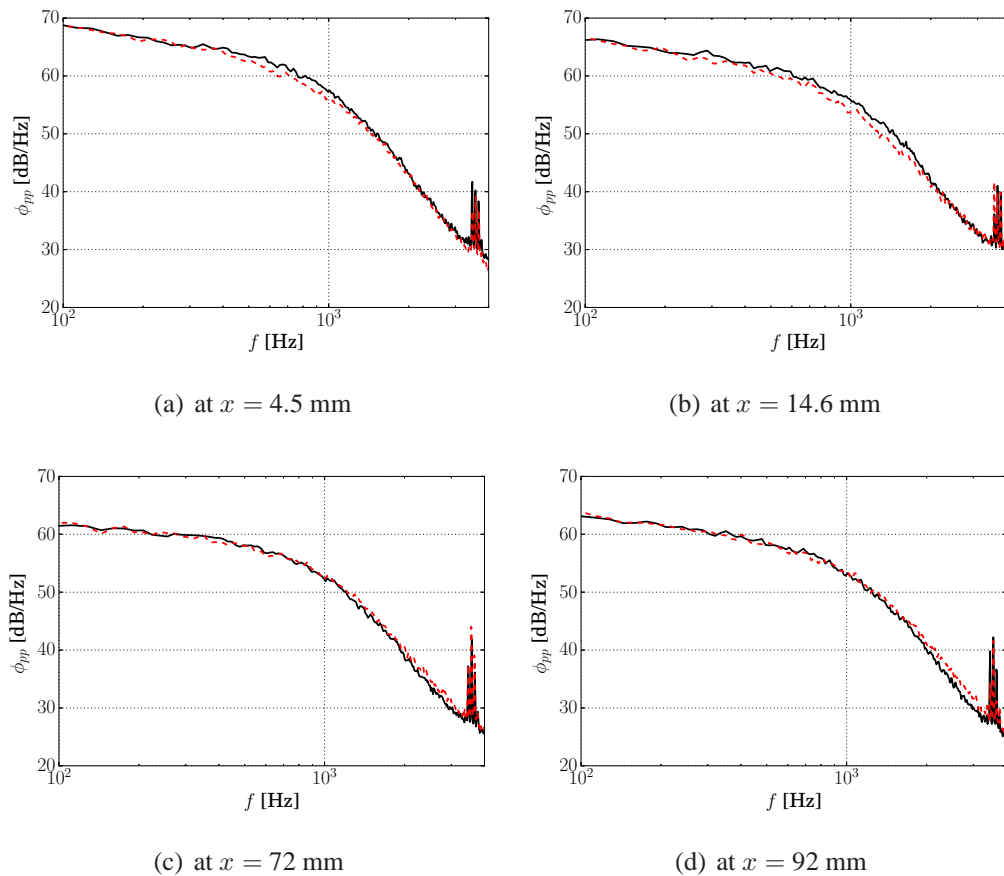

(c) at $x = 72$ mm

(d) at $x = 92$ mm

Figure 6: Point spectra of pressure fluctuations; – no TE case, – – TE case

around 3 kHz are due to the tonal noise components of the wind tunnel fan. The captured $\phi_{pp}(f)$ are quite similar to each other at the first two streamwise locations (Fig. 6(c) and (d)). There is a more pronounced difference between the dashed red and solid black curves around 1 kHz at $x = 4.5$ and 14.6 mm, which corresponds to the hydrodynamic range. One can conclude that the presence of the TE causes distortion on the power spectra of the pressure fluctuations, see Fig 6(a) and (b). To better understand the change in the pressure spectra, further measurements are required to resolve the spatial part of ϕ_{pp}.

The last calculated input property of the TE models is the spanwise length scale of the turbulent eddies (Λ_3, see Eq. 10), which is presented in Fig. 7. The figure shows that no significant change was experienced in the spanwise length of the structures, which means that this property was not affected by the presence of the trailing edge.

Up until this point, the main properties of the boundary layer and the pressure point spectra has been presented, most of which are used as input parameters for the TE noise models. As a final step, the second order quantities and correlation properties are presented and discussed. The first quantity to consider is the correlation coefficient (r) between the surface pressure fluctuations and the velocity fluctuations within the boundary layer, which is plotted as a function of y^+ in Fig. 8(a). The correlation coefficient was calculated at the last streamwise microphone location ($x = 4.5$ mm) and the highest presented y^+ corresponds to $y/\delta = 1.5$. The plot shows that the correlation coefficient decreases over the entire boundary layer in the presence of a TE.

Figure 8(b) presents the change in magnitude square coherence ($\Delta\gamma^2$) between the hot-wire and the microphone data along the boundary layer. The property shows the change between the TE and the no TE cases, i.e. $\Delta\gamma^2 = \gamma^2_{TE} - \gamma^2_{noTE}$. While the correlation coefficient (r) decreased in the entire boundary layer, the magnitude squared coherence increases, which is clearly visible in Fig. 8(b). The highest increase was experienced in the low frequency region ($\approx$100–300 Hz) and close to the
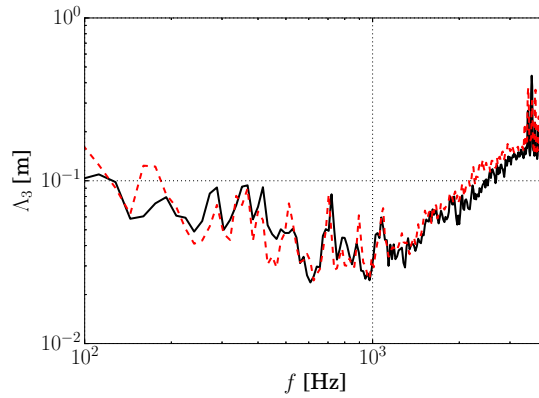
Figure 7: Spanwise length scale of turbulent structures; – no TE case, – – TE case

wall ($x/\delta < 0.1$). Further experiments are planned to investigate the importance of the v velocity component in this phenomena.
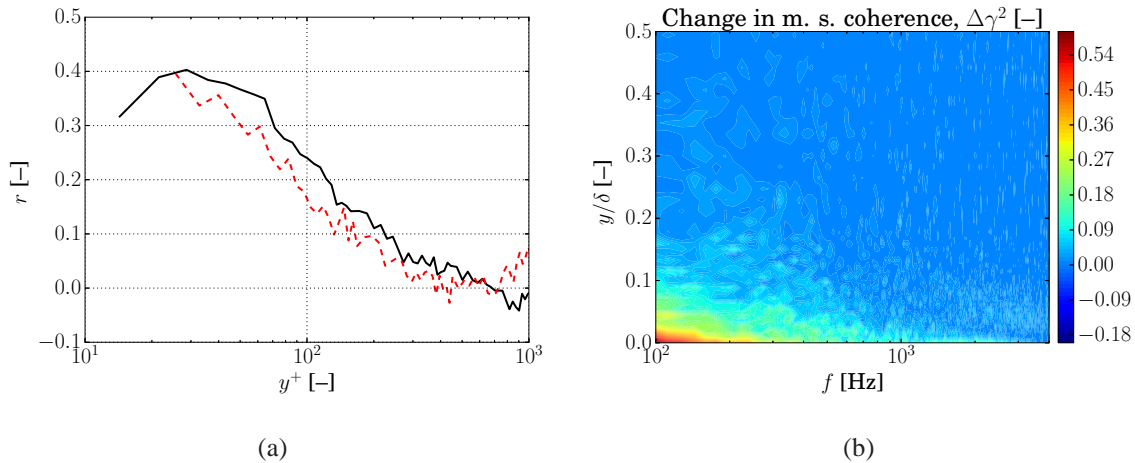

(a)

(b)

Figure 8: Second order properties: (a) Pearson's correlation coefficient and (b) change in magnitude squared coherence between u' and p' above the last microphone location; – no TE case, – – TE case

The temporal cross correlation along the boundary layer as a function of the dimensionless time shift ($R_{u'p'}(y, \tau) = u'(y, t + \tau)p'(t)/(u_{RMS}\, p_{RMS})$) is presented for the cases when the TE was not (Fig. 9(a)) and was (Fig. 9(b)) present in the flow. We can see lower amplitudes of $R_{u'p'}$ in Fig. 9(b) compared to Fig. 9(a), i.e. the red coloured area is smaller in both time and in space domain for the TE case. This observation implies that smaller structures present in the flow close to the TE. It can be concluded from the smaller time extent of this area in Fig. 9(b) that the corresponding frequency of the dominant eddies are decreased in the TE case. The decreased extent of the turbulent structures for the TE case also indicates that the eddies are more likely to be found in the lower region of the BL than in the outer region. The horizontal streaks in Fig. 9(b) suggests that the eddies are elongated by the presence of the TE, which assumption will be further investigated in the upcoming measurements.

5. Summary

This paper investigates the uncertainty of three different trailing edge (TE) noise models, namely the BPM [5], the TNO [4] and Amiet model [3] with the help of the measurement of their input properties. The measurement of the u velocity component and the surface pressure fluctuation was performed for the cases when TE was and was not present in the flow. It was found that the majority
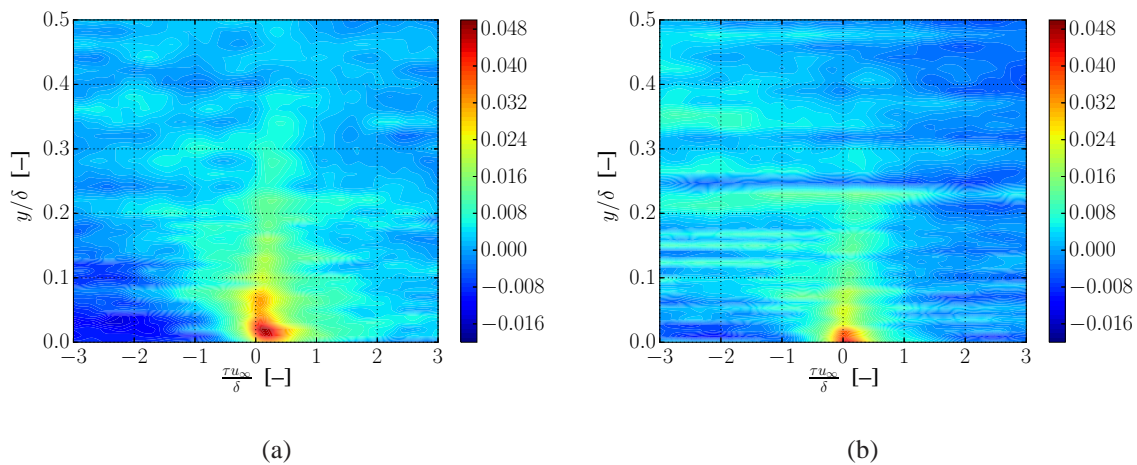
Figure 9: Temporal cross correlation of velocity and pressure fluctuations above the last microphone: (a) no TE case, (b) TE case

of the investigated properties change in the vicinity of the TE. This implies that as the flow approaches the TE, these quantities begin to deviate from the properties of an ideal boundary layer. Since these models rely on ideal BL properties, this introduces uncertainty in the calculation of the TE noise.

It was shown that the wall shear stress increases, the energy content of the streamwise velocity decreases and the amplitude of the point spectra of the surface pressure fluctuations also decrease as the flow approaches the TE. The integral properties and the friction velocity along the plate are also affected by the presence of the TE. On the other hand, it was found that the streamwise extent of the turbulent structures does not change significantly when the trailing edge is present.

Based on the measured quantities in the study, it is shown that the trailing edge has a non negligible distortion effect on the flow properties, and further measurements involving hot-film and cross-wire are required in order to more accurately quantify the effect of the trailing edge on the flow.

References

1. Howe, M. A review of the theory of trailing edge noise, *Journal of Sound and Vibration*, **61**, 437–465, (1978).

2. Blake, W. K., *Mechanics of flow-induced sound and vibration V2: Complex flow-structure interactions*, Elsevier (2012).

3. Amiet, R. K. Noise due to a turbulent flow past a trailing edge, *Journal of Sound and Vibration*, **47**, 387–393, (1976).

4. R. R. Parchen and Technisch Physisce Dienst. Progress report draw: A prediction scheme for trailing edge noise based on detailed boundary layer characteristics, *TNO Report*, **HAG-RPT-980023**, (1998).

5. Brooks, T. F., Pope, D. S. and Marcolini, M. A. Airfoil self-noise and prediction, *NASA Report*, (1989).

6. Roger, M. and Moreau, S. Trailing edge noise measurements and prediction for subsonic loaded blades, *AIAA Journal*, **AIAA-2002-2460**, (2002).

7. Liu, X., Azarpeyvand, M. and Theunissen, R. Aerodynamic and aeroacoustic performance of serrated airfoils, *21st AIAA/CEAS Aeroacoustics Conference*, **AIAA 2015-2201**, (2015).

8. Ai, Q., Azarpeyvand, M., Lachenal, X. and Weaver, P. M. Aerodynamic and aeroacoustic performance of airfoils with morphing structures, *Wind Energy*, we.1900, (2015).

9. Lyu, B., Azarpeyvand, M. and Sinayoko, S. Prediction of noise from serrated trailing edges, *Journal of Fluid Mechanics*, **793**, 556–588, (2016).

10. Azarpeyvand, M., Gruber, M. and Joseph, P. F. An analytical investigation of trailing-edge noise reduction using novel serrations, *19th AIAA/CEAS Aeroacoustics Conference*, **AIAA 2013-2009**, (2013).

11. Ai, Q., Azarpeyvand, M., Lachenal, X. and Weaver, P. M. Airfoil noise reduction using morphing trailing edge, *21st International Congress on Sound and Vibration*, (2014).

12. Liu, X., Jawahar, H. K., Azarpeyvand, M. and Theunissen, R. Wake development of airfoils with serrated trailing edges, *22nd AIAA/CEAS Aeroacoustics Conference*, (2016).

13. Perarson, K. Notes on regression and inheritance in the case of two parents, *Proceedings of the Royal Society of London*, **58**, 240–242, (1895).